Prediction of surface currents and drifter trajectories on the inner Scotian Shelf

Keith R. Thompson, Jinyu Sheng, Peter C. Smith,[1] and Liangzi Cong
Department of Oceanography, Dalhousie University, Halifax, Nova Scotia, Canada

Received 27 August 2001; revised 29 November 2001; accepted 27 February 2003; published 5 September 2003.

[1] The predictive skill of a simple model of surface flow on the Scotian Shelf is assessed using oceanographic data collected in February 1996. The model is forced by wind stress, water density, and sea level along the open boundaries of the model domain. The skill of the model with respect to subtidal variations of alongshore current and bottom pressure is quantified by the ratio $\gamma^2 = \mathrm{Var}(O - P)/\mathrm{Var}(O)$, where $\mathrm{Var}(O - P)$ and $\mathrm{Var}(O)$ are the variance of the prediction errors and observations, respectively. Skill is highest for bottom pressure ($\gamma^2 = 0.2$) followed, in order, by cross-shelf gradients in bottom pressure ($\gamma^2 = 0.5$), horizontally averaged currents ($0.4 < \gamma^2 < 0.7$), and currents at individual current meters ($0.6 < \gamma^2 < 1.4$). The skill of the model with respect to drifter position is quantified by the search radius, centered on the predicted drifter position, that ensures a 50% chance of locating the drifter. Skill varies significantly with time but is generally highest when the drifter motion is strongest. We conclude with a comparison of the performance of the model against predictions based on the release point of the drifters and the operational scheme presently used to guide marine search and rescue in this region. *INDEX TERMS:* 4255 Oceanography: General: Numerical modeling; 4512 Oceanography: Physical: Currents; 4263 Oceanography: General: Ocean prediction; *KEYWORDS:* shelf circulation, drifter trajectories, prediction skill

Citation: Thompson, K. R., J. Sheng, P. C. Smith, and L. Cong, Prediction of surface currents and drifter trajectories on the inner Scotian Shelf, *J. Geophys. Res.*, *108*(C9), 3287, doi:10.1029/2001JC001119, 2003.

1. Introduction

[2] There is growing interest in operational models that can nowcast and forecast near-surface currents on the continental shelf. Such models could be used, for example, to predict oil spill and iceberg trajectories and guide marine search-and-rescue missions. The present study is part of an ongoing effort to construct a coastal ocean forecast system for the eastern seaboard of Canada.

[3] We assess the skill of a prototype operational model of the Scotian Shelf that is presently under development at Dalhousie University. The time-varying component of the flow is predicted by a three dimensional, linear, barotropic model. It is forced at the sea surface by wind stress. Coastal sea level is used to infer the time-varying conditions along the open boundary through which coastal trapped waves enter the model domain. The mean component of the surface flow is diagnosed from all hydrographic data available for the Scotian Shelf. The resulting mean surface drift is to the southwest and is believed to be part of a basin-scale, buoyancy-driven flow that connects the Labrador Shelf, Gulf of St. Lawrence, Gulf of Maine and Mid Atlantic Bight [e.g., *Smith and Schwing*, 1991]. This diagnosed mean flow is the background state to which the barotropic model solution relaxes in the absence of forcing.

[4] The observations used to validate the model were made on the inner Scotian Shelf in February 1996. They include coastal sea levels, bottom pressures, currents at fixed moorings, temperatures and salinities and the trajectories of drifters released in four trials each of about one week's duration. (Details of the field program are given by *Sheng et al.* [2001] along with a description of the observations.)

[5] We will show that the model has significant skill in predicting currents, in accord with an earlier analysis by *Thompson and Sheng* [1997] of data collected in the same region during the Canadian Atlantic Storm Program (CASP) in the winter of 1985–1986. The present study differs from the earlier CASP analysis by including drifter trajectories in the validation data set. It is generally accepted that drifter trajectories are more difficult to predict than currents and provide a severe test of any circulation model.

[6] We review the field program and observations in the next section and describe the circulation model in Section 3. Model predictions and observations are compared in Section 4. The sensitivity of the model predictions to changes in vertical eddy viscosity, bottom friction and the horizontal resolution of the wind are described in Section 5. Conclu-

[1] Also at Bedford Institute of Oceanography, Dartmouth, Nova Scotia, Canada.

0148-0227/03/2001JC001119

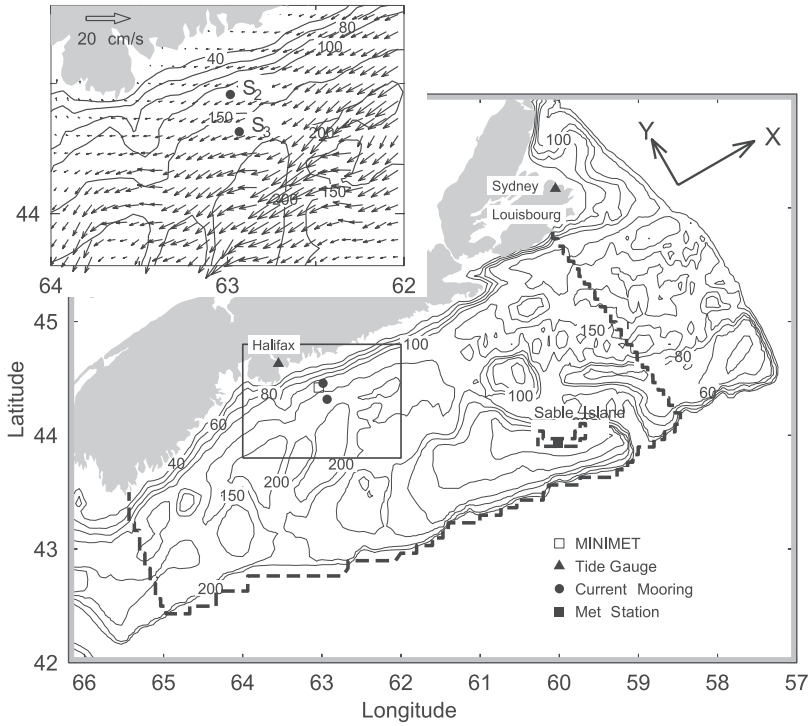

Figure 1. Main bathymetric features of the Scotian Shelf, the locations of the instruments, and the model domain. The contours show water depth in meters. The dashed line shows the open boundaries of the barotropic model. The inset shows the surface baroclinic flow in the vicinity of moorings S2 and S3 that was diagnosed from density profiles observed on the Scotia Shelf. The MINIMET meteorological buoy is close to S2, and the meteorological station is on Sable Island. Alongshore currents are positive toward 65°T.

sions are given in the final section along with suggestions for further work.

2. Observations

[7] The main objective of the field program was to evaluate the skill of the existing operational search planning system for the region (Canadian Search and Rescue Planning (CANSARP)) and to increase accuracy through the use of higher-resolution winds and a better circulation model.

[8] Five types of drifter were deployed on the inner Scotian Shelf (Figure 1) in four trials, each of about one week's duration in February 1966. The Accurate Surface Tracker (AST) is a barrel drifter with an 80 cm draft and a small mast. Its drift characteristics are know to resemble those of a person-in-water. The Convertible Accurate Surface Tracker (CAST) was equipped with 12 m holey sock drogue centered at 15 m. These buoys are designed to track near surface currents, excluding the effects of leeway and the surface wind drift layer. A small dory, tethered to an AST for tracking, and six-person and four-person life rafts were also used as drift objects. Most of the ASTs had internal GPS receivers that provided hourly positions with an accuracy of 10 m. The remaining drift objects used ARGOS positioning at an irregular rate and an accuracy of about 150 m. (For further details on the drifters, see *Smith et al.* [1998].)

[9] Two moorings, each with three current meters, were placed on the 100 m and 165 m isobaths (moorings S2 and S3 respectively, see Figure 1 and Table 1). Sea level was recorded at Halifax and bottom pressure was recorded at S2 and S3. All current, sea level and bottom pressure records were low-pass filtered (cutoff period of 27 hours) to remove the diurnal and semidiurnal tides. Local wind measurements were made by an anemometer on a surface meteorological buoy anchored adjacent to S2. Cross-shelf lines of hydrographic stations were run during the deployment and recovery cruises for each of the four drifter trials. This allowed an estimate to be made of the variability in the density field and hence the baroclinic component of flow. More detailed descriptions of the experimental procedures and observations are given by *Sheng et al.* [2001].

[10] The wind fields used to drive the model were provided by the Canadian Meteorological Centre. The fields were calculated using a regional finite element atmospheric model run at 35 km and 12 km horizontal resolution. Both sequences of wind fields were comprised of 6 h and 12 h forecasts made twice daily. The fields were linearly interpolated to the model time step of 50 s, and then interpolated onto the model grid using a four point bivariate interpolation scheme [*Abramowitz and Stegun*, 1970, p. 882].

[11] To check the accuracy of the wind fields they were compared against the winds observed at the meteorological buoy adjacent to S2 (Figure 2). There is clearly quite good agreement between the observed and forecast winds. Figure 2 also shows that the differences between

Table 1. Statistics of Observed and Predicted Flow Variability at S2 and S3[a]

		s_u		$s_u^2/(s_u^2 + s_v^2)$					
Mooring	Depth, m	Observed	Predicted	Observed	Predicted	β_1	r^2	$1-r^2$	γ^2
S2	16	6.0	8.3	0.60	0.97	0.47	0.42	0.58	1.12
S2	50	4.4	7.1	0.50	0.98	0.43	0.47	0.53	1.35
S2	70	5.0	6.9	0.75	0.97	0.60	0.68	0.32	0.63
S3	16	6.5	6.5	0.30	0.88	0.66	0.43	0.57	0.68
S3	70	5.1	4.2	0.42	0.69	0.75	0.37	0.63	0.67
S3	110	4.7	4.4	0.60	0.73	0.60	0.31	0.69	0.83
S2 + S3	16	5.5	7.3	0.40	0.95	0.60	0.63	0.37	0.65
S2 + S3	70	4.6	5.4	0.57	0.89	0.68	0.66	0.34	0.48

[a]The standard deviation of the alongshore flow is denoted by s_u and given in cm s^{-1}. The statistic $s_u^2/(s_u^2 + s_v^2)$ is the ratio of the variance of the alongshore current to the total current variance, $s_u^2 + s_v^2$. Both statistics are presented for the observations and predictions. The regression coefficient (β_1) and squared correlation (r^2) from the regression of observed on predicted alongshore flow ($u_{obs} = \beta_0 + \beta_1 u_{pred} + \epsilon$) are given in columns 7 and 8. The last column is more direct measure of model fit, $\gamma^2 = \mathrm{Var}(u_{obs} - u_{pred})/\mathrm{Var}(u_{obs})$.

the 35 km and 12 km wind are small at the meteorological buoy.

3. Circulation Model

[12] The surface flow is assumed to be the linear superposition of a seasonal mean baroclinic component, diagnosed from observed density profiles, and a barotropic component forced by local wind stress and flow through the model's open boundaries. Some justification for this assumption is given by *Thompson and Sheng* [1997]. The use of more complex models is discussed in Section 6.

3.1. Baroclinic Component

[13] The mean surface flow was diagnosed from density observations using the method proposed by *Sheng and Thompson* [1996]. The method is based on the separation of bottom density into two parts: $\rho_h = \tilde{\rho}_h + \rho_h'$ where $\tilde{\rho}_h$ is bottom density averaged along isobaths of depth h, and $\rho_h'(x,$

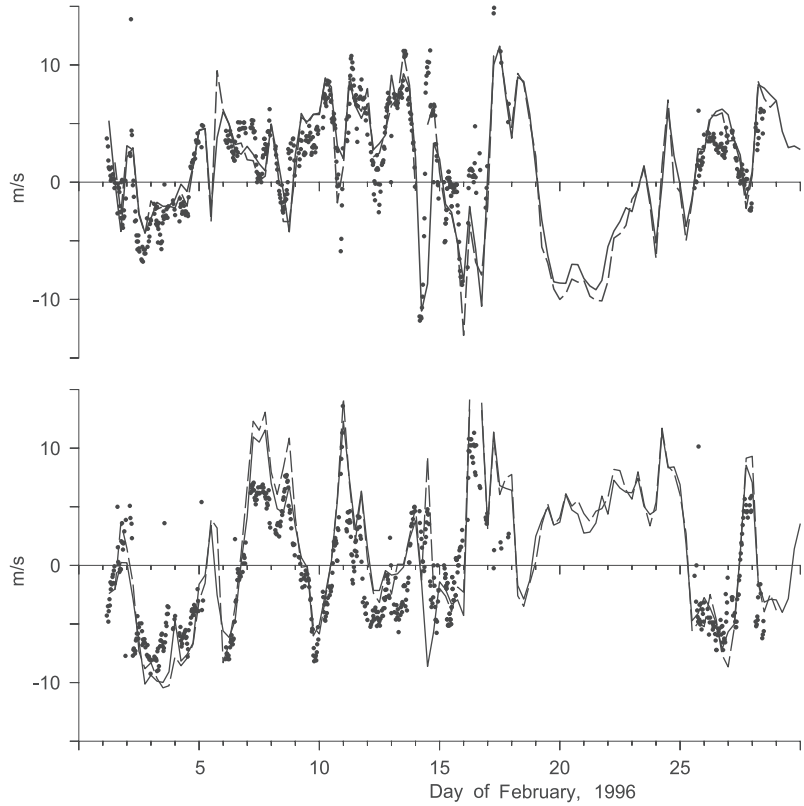

Figure 2. Validation of the wind fields used to drive the barotropic model. The dots show the winds recorded at a height of 2 m by the anemometer on the surface meteorological buoy. Note the failure of the anemometer between 18 and 25 February. The solid (dashed) line shows the surface wind from the 35 km (12 km) atmospheric models, interpolated to the anemometer position. The top panel is for an eastward wind, and the bottom panel is for a northward wind. Winds are in m s^{-1}.

y) is the local deviation about this mean. This allows sea level η, and hence the surface geostrophic flow, to be decomposed in a similar way: $\eta = \tilde{\eta} + \eta'$ where $\tilde{\eta}$ is dynamic height relative to a deep, spatially invariant reference level and η' is a correction term. The dynamic height $\tilde{\eta}$ depends only on the vertical density profile at a given point and its extrapolation from the seafloor to the deep reference level by $\tilde{\rho}_h$. The correction η' satisfies a two-dimensional elliptic partial differential equation forced by ρ'_h. Before calculating η' we first examine the spatial structure of the point measurements of ρ'_h and test if they are statistically different from uncorrelated noise. If they are indistinguishable from noise, the correction term is set to zero and sea level is approximated by $\tilde{\eta}$. Thus the method has a degree of robustness to errors in the density observations. If the ρ'_h have well-defined spatial structure the elliptic equation is solved for η' and sea level is equated to $\tilde{\eta} + \eta'$. Note even if the calculation of η' is required, the only gridding of the density data is two dimensional. This method is therefore simpler to use than many of the existing diagnostic models which require three-dimensional gridding of the observed density profiles.

[14] The density observations used in the present study include all vertical density profiles collected on the Scotian Shelf over the last 70 years during winter, including profiles collected during February 1996. The diagnosed flow pattern captures the main features of the winter mean circulation in this region including a overall drift to the southwest of about 0.1 m s^{-1} and the Nova Scotia Current, an alongshore baroclinic jet centered on the 200 m isobath close to shore (inset of Figure 1).

3.2. Barotropic Component

[15] The linearized horizontal momentum and continuity equations governing barotropic flow on the continental shelf are taken to be

$$\frac{\partial \vec{u}}{\partial t} + \vec{f} \times \vec{u} = -g\nabla\eta + \frac{\partial}{\partial z}\left(\mu \frac{\partial \vec{u}}{\partial z}\right) \tag{1}$$

and

$$\frac{\partial \eta}{\partial t} + \nabla \cdot \int_h^0 \vec{u} dz = 0 \tag{2}$$

where $\vec{u} = (u, v)$ is the horizontal flow vector, f is the Coriolis parameter, g is acceleration due to gravity, η is the height of the sea surface relative to its undisturbed level, μ is the vertical eddy viscosity and h is water depth. The top and bottom boundary conditions are

$$\mu \frac{\partial \vec{u}}{\partial z} = \begin{cases} \vec{\tau}/\rho_0 & z = 0 \\ k\vec{u} & z = -h \end{cases} \tag{3}$$

where $\vec{\tau}$ is the wind stress, ρ_0 is a reference water density and k is a bottom friction coefficient.

[16] To calculate η and $\vec{u}$, we follow *Sheng and Thompson* [1993] and subtract the steady Ekman flow, $\vec{u}_E$, from $\vec{u}$. The remainder, $\vec{u}_R = \vec{u} - \vec{u}_E$, satisfies (1) and (2) with the terms $\partial \vec{u}_E/\partial t$ and $\nabla \cdot \int_{-h}^0 \vec{u}_E dz$ subtracted from the right-hand side of (1) and (2) respectively. The remainder $\vec{u}_R$ is expanded in terms of eddy viscosity eigenfunctions, i.e., the solutions to a Sturm Liouville problem based on

$$\frac{\partial}{\partial z}\left(\mu \frac{\partial \phi}{\partial z}\right) + \lambda\phi = 0, \tag{4}$$

where ϕ is an eddy viscosity eigenfunction and λ the associated eigenvalue. The top and bottom boundary conditions for $\vec{u}_R$, and ϕ, are given by (3) with $\vec{\tau}$ set to zero. This ensures rapid convergence of the eigenfunction expansion. On the basis of the work of *Thompson and Sheng* [1997] we chose 10 eigenfunctions as a compromise between vertical resolution and computational efficiency. We also assumed μ to be constant with depth. The sensitivity of the model predictions to changes in μ is discussed in Section 5.

[17] The initial condition is a state of rest. We estimate the spin-up time of the barotropic model to be about one day and so the initial condition is relatively unimportant in the present study which involves integrations of about one month.

[18] At the coastal boundary we require the normal transport to be zero. The offshore boundary coincides approximately with the 200 m isobath (Figure 1) and the sea level there is set to zero. This is based on the belief that the continental slope insulates the shelf from the influence of low-frequency barotropic flow in the adjacent deep ocean [e.g., *Wright et al.*, 1986]. Sensitivity studies designed to explore the influence of the deep ocean on Scotian Shelf circulation are discussed by *Thompson and Sheng* [1997].

[19] Along the western cross-shelf boundary we use an *Orlanski* [1976] boundary condition with the modification of *Miller and Thorpe* [1981]. The result is a forward-in-time, upstream differencing of the Sommerfeld radiation condition with the local phase speed estimated from state values at grid points close to the open boundary. It has been shown [*Chapman*, 1985] that this boundary condition rapidly damps sieching of the interior while retaining the correct low-frequency wind-driven response.

[20] At the eastern boundary we assume sea level drops linearly with distance from shore, ranging from a coastal value denoted by η_L to zero at the shelf break [*Thompson and Sheng*, 1997]. The nearest tide gauge to the eastern boundary was at Sydney (Figure 1). Unfortunately its sea level record had many gaps during February 1966 and so we used the following ad hoc method for estimating η_L from the continuous Halifax record for February 1996.

[21] Halifax sea level, η_H, was first expressed as the sum of four components:

$$\eta_H = \eta_a + \eta_w + \eta_d + \eta_r. \tag{5}$$

The inverse barometer effect, η_a, was calculated in the usual way from local air pressure. The wind effect, η_w, was calculated by forcing the barotropic model with winds over the Scotian Shelf and setting sea level at the eastern boundary to zero. The Halifax sea level record, after removal of the inverse barometer and wind effect, is shown in Figure 3a.

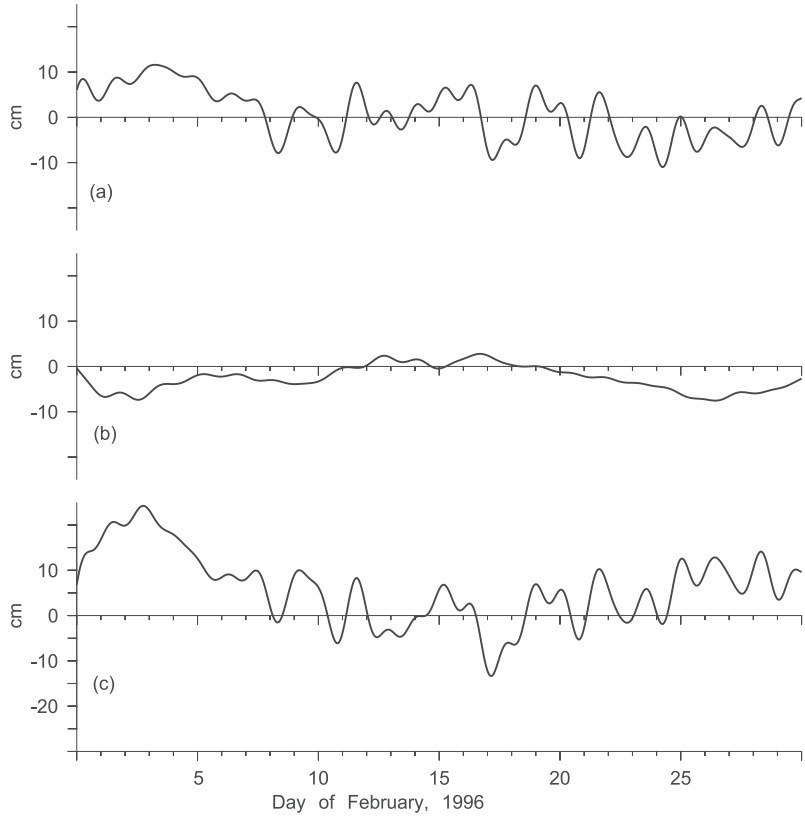

Figure 3. Decomposition of Halifax sea level. (a) Halifax sea level, η_H, after removal of the effect of air pressure, η_a, and local wind, η_w (b) Density contribution, η_d, and (c) residual sea level, $\eta_H - \eta_a - \eta_w - \eta_d$. Sea levels are in cm.

[22] The time-varying effect of water density offshore of Halifax was calculated using

$$\eta_d = \frac{1}{\rho_0} \int_h^0 \rho_h dh \tag{6}$$

where ρ_0 is a reference density, ρ_h is the bottom density and h is the water depth [*Csanady*, 1979]. Five shore normal density sections were made during the field program which allowed five estimates of η_d to be made using (6). To convert these point estimates into a continuous record, we regressed the five point estimates of η_d on the five contemporaneous bottom temperatures measured at S3. The slope of the best fitting straight is -2.34 cm $^\circ C^{-1}$ and the regression accounted for 58% of the variance of η_d. This linear relationship was then used to convert the continuous bottom temperature record from S3 into a continuous record of η_d (Figure 3b).

[23] The final step was to assume η_r (Figure 3c) is caused by remotely generated, coastal trapped waves that enter the model through the eastern boundary. To infer the eastern boundary condition that generated η_r we ran the barotropic model with (i) wind stress set to zero, and (ii) an eastern boundary condition based on an historical sea level record from Louisbourg (Figure 1) which is close to the shoreward end of the eastern boundary. (Unfortunately sea level data were not available from Louisbourg for February 1996.) From this run we found that, on average, predicted Halifax sea level lags η_L by 4.0 hours and is attenuated by a factor of 0.65. Thus to recover coastal sea level at the eastern boundary from η_r, and hence the time-varying eastern boundary condition for February 1966, we shifted η_r by 4 hours and scaled it by $1/0.65 \approx 1.54$.

[24] The horizontal grid spacing of the barotropic model is 5.4 km in the east-west direction and 7.5 km in the north-south direction. For our standard run we took $\mu = 204$ cm^2 s^{-1}, $k = 0.15$ cm s^{-1} and forced the model with the 35 km winds. The sensitivity of the predicted flow to changes in μ, k and wind resolution is discussed in Section 5.

4. Model Validation

[25] Let Var(O) denote the variance of observed alongshore current or bottom pressure and let Var(O-P) denote the variance of the corresponding prediction error. The skill of the model with respect to these two variables is measured by the ratio

$$\gamma^2 = \frac{\mathrm{Var(O - P)}}{\mathrm{Var(O)}}. \tag{7}$$

In general the smaller γ^2 the higher the skill of the model. If subtraction of the model's predictions from the observations reduces error variance then γ^2 is less than unity. Conversely,

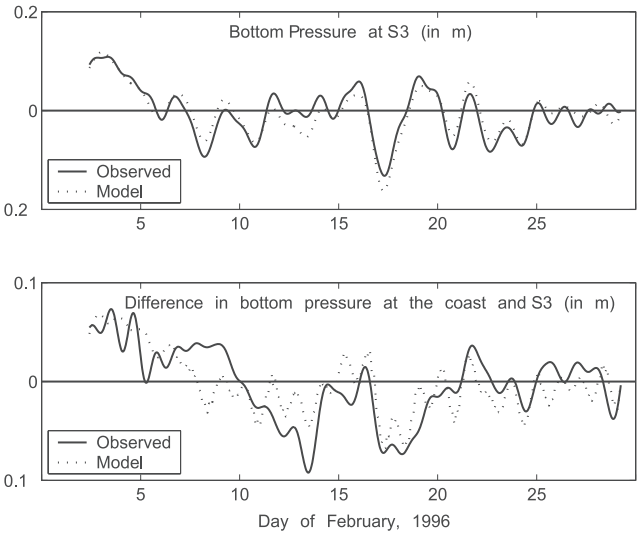

Figure 4. Comparison of observed and predicted bottom pressure. The top panel shows bottom pressure at S3. The bottom panel shows the difference in Halifax sea level and bottom pressure at S3. Observed Halifax sea level was adjusted for the effect of air pressure and density as described in the text. The means of all series have been removed and the units are m.

if γ^2 exceeds unity the mean (or any other constant value) is a more effective predictor of the observed variability than the circulation model. The γ^2 statistic is less forgiving than a simple correlation between observations and predictions. If, for example, the model is perfect except for a systematic under or over prediction by a constant factor δ, the correlation between observations and predictions will be unity but γ^2 will equal $(1 - \delta)^2$.

4.1. Bottom Pressure

[26] The agreement between observed and predicted coastal sea level at Halifax is excellent. This agreement is however not surprising because the eastern boundary condition is inferred from Halifax sea level. It is also not surprising to find good agreement between observed and predicted bottom pressure at S3, which is only about 50 km from Halifax ($\gamma^2 = 0.18$, Figure 4 (top)).

[27] A more critical test of the model is its ability to predict the gradient in bottom pressure across the shelf. The solid line in the lower panel of Figure 4 shows the difference in observed Halifax sea level, after correction for air pressure and density, and bottom pressure at S3. This spatial difference varies by more than 10 cm over the course of the field program implying variations in alongshore geostrophic flow of order 10 cm s^{-1}. The dotted line in the lower panel shows the changes predicted by the barotropic model. Encouragingly the observed and predicted differences are quite similar ($\gamma^2 = 0.54$).

4.2. Currents

[28] The means of the near-surface currents observed at S2 and S3 are almost alongshore with speeds of 4.3 and 11.7 cm s^{-1} respectively (Table 2). The predicted means vary less between moorings compared to the observations (Table 2). The predicted means are due entirely to the diagnosed baroclinic component. (The barotropic component is required to have zero mean because we do not know the absolute datums of the Halifax tide gauge and can infer only variations in flow). The similarity of the predicted means at S2 and S3 is therefore related to the horizontal smoothing of the hydrographic data that was required to infer reliable baroclinic flows.

[29] Although the agreement between observed and predicted mean alongshore flow at individual current meters is only fair, it improves in both along and cross-shore directions if currents from the two moorings are averaged (last row of Table 2). Note that both observations and predictions have relatively weak cross-shore flows, everywhere less than 2 cm s^{-1}. We conclude that the model is giving a reasonable prediction of the mean flow on spatial scales exceeding 15 km, (the distance between S2 and S3).

[30] Turning now to the subtidal variability, the standard deviation of the observed alongshore flow ranges between 4.4 and 6.5 cm s^{-1} in (s_u, Table 1). At the near-surface and middepth meters on S3 the cross-shore variations are stronger than the alongshore variations ($s_u^2/(s_u^2 + s_v^2) < 0.5$, Table 1). The predicted currents are more rectilinear than the observations, the result of topographic steering of the subtidal barotropic flow. The following discussion of model performance will focus on the alongshore component.

[31] The skill of the model with respect to variations in alongshore flow ranges from $\gamma^2 = 0.63$ at the 70 m current meter on S2, to $\gamma^2 = 1.35$ at the 50 m current meter on the same mooring (Table 1). The time series plots of observed and predicted alongshore currents (not shown) suggest that the reason for the high γ^2 (poor fit) at S2 may be over prediction of the alongshore flow. To check, the observed alongshore flow was regressed on the corresponding model prediction using a linear regression model of the form $\hat{u}_{obs} = \beta_0 + \beta_1 u_{pred}$. Scaling the model predictions by the optimal amount (β_1, Table 1) reduces γ^2 at S2 to between 0.3 and 0.6, ($1-r^2$, Table 1) confirming the model is overpredicting the alongshore flow at this mooring. The over prediction is not as pronounced at S3 where γ^2 is reduced by about 0.1 at all meters (compare the last two columns of Table 1).

[32] One reason considered for the over prediction of alongshore flow was an underestimation of the bottom drag coefficient, k. This would result in a wind-driven, frictional boundary layer that is too narrow [see, e.g., *Csanady*, 1982, p. 198]. In fact a plausible increase in k would reduce the predicted flow at both moorings with the largest change at S2 as observed. This cannot be the complete explanation however because it cannot account for the depth depen-

Table 2. Means of Observed and Predicted Near-Surface Flow at S2 and S3[a]

	$\bar{u}$		$\bar{v}$	
Mooring	Observed	Predicted	Observed	Predicted
S2	−4.3	−7.3	−1.7	−0.2
S3	−11.7	−6.3	1.6	−1.3
S2 + S3	−8.0	−6.8	−0.0	−0.7

[a]Means in the alongshore and cross-shore direction are denoted by $\bar{u}$ and $\bar{v}$ respectively. The row labelled S2 + S3 is the vector mean of the flows at S2 and S3. The depth of the meters is 16 m. The data cover the period 1–28 February 1996.

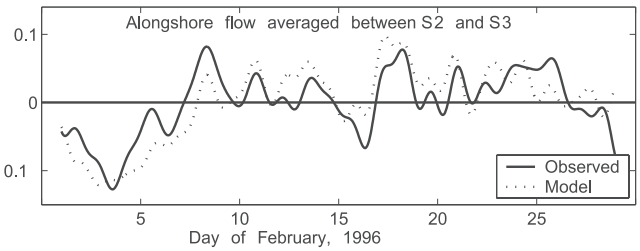

Figure 5. Along-shore currents at the midpoint between S2 and S3 at a depth of 70 m. Currents are in m s^{-1}.

dence of the over prediction. We return to this point is Section 5.

[33] Observed current variations at the same depth are less similar than the corresponding predictions. (For example, the squared correlation between the observed alongshore currents at 16 m at S2 and S3 is $r^2 = 0.41$; the corresponding r^2 for the predictions is 0.87.) It is therefore of interest to ask if spatial averaging of the currents will improve model fit. Spatially averaging observations and predictions at S2 and S3 decreases γ^2 to 0.65 at 16 m and 0.48 at 70 m (last two rows of Table 1). Again we conclude that model skill is higher on scales exceeding 15 km. Plots of the observed current at 70 m, averaged over S2 and S3, and the corresponding model predictions are shown in Figure 5.

4.3. Drifter Trajectories

[34] The trajectory of a surface drifter which was at $\vec{x}_0$ at time t_0 was obtained by solving

$$\frac{d\vec{x}(t)}{dt} = \vec{u}(\vec{x}, t) + a\vec{w}(\vec{x}, t) \tag{8}$$

subject to

$$\vec{x}(t_0) = \vec{x}_0$$

where $\vec{x}(t)$ is the horizontal position of the drifter at time t, $\vec{u}(\vec{x}, t)$ is the model velocity, $\vec{w}(\vec{x}, t)$ is the 10 m wind and α is a leeway factor. The product $\alpha\vec{w}$ is therefore the velocity of the drifter with respect to the surface current.

[35] Leeway factors have been estimated in various ways. For example, *Smith* [1992] describes a set of experiments using ASTs in which α is parameterized in terms of the ratio of exposed to submerged frontal areas. Using this parameterization we estimate a leeway factor of 0.005 ± 0.001. This estimate does not account for the contribution of the

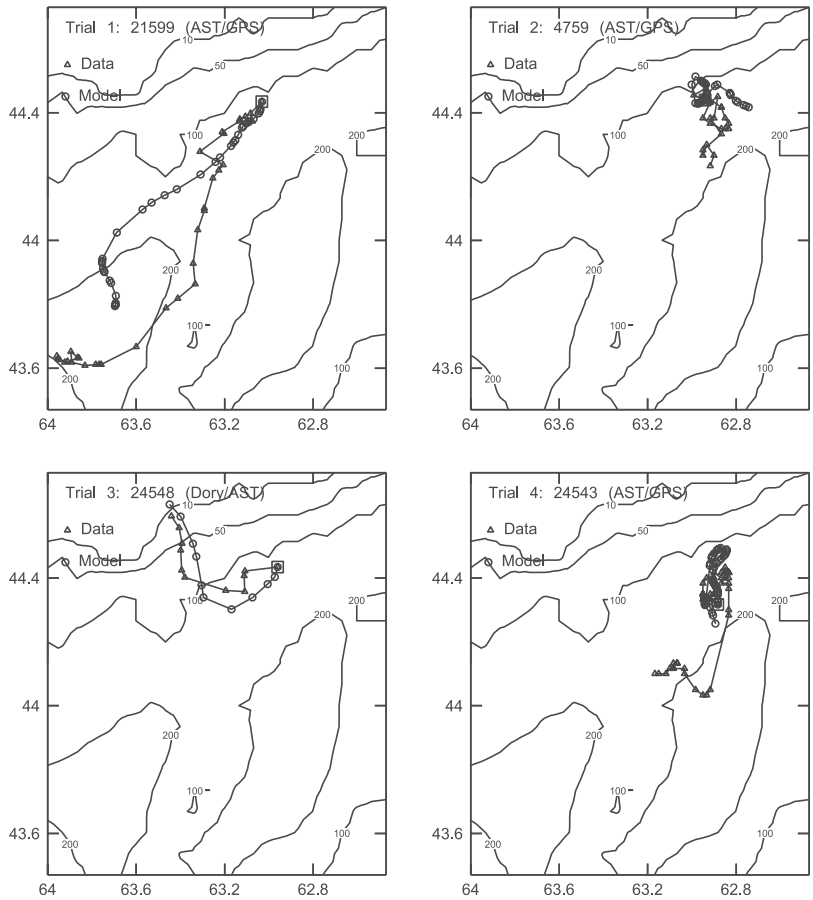

Figure 6. Pairs of observed and predicted drifter trajectories for each of the four trials. The observed positions are shown by triangles, and the predicted positions are shown by circles. The sampling interval is irregular but on the order of 6 hours.

Table 3. Leeway Factors

Drifter Type	α
AST	0.008 ± 0.001
Life raft with drogue	0.02
Life raft without drogue	0.036 ± 0.002
Dory	0.037 ± 0.005
CAST with drogue	0

wind drift layer which includes the surface log layer [*Csanady*, 1984]. Using the approach of *Csanady* [1984], we calculated that the wind drift current acting on an AST could be approximated by 0.003 $\vec{w}$. The result is a leeway factor for ASTs of $\alpha = 0.005 + 0.003 = 0.008$. Leeway factors for dory and life rafts were based on direct measurements made during Canadian Coast Guard trials on the Grand Banks [*Oceans Ltd.*, 1994]. The CAST, which is drogued at 15 m, was assumed to track the current at that level with no leeway correction. A summary of the leeway factors used in this study is given in Table 3.

[36] Typical trajectories for each of the four trials are shown in Figure 6. It is clear from this figure that there is qualitative agreement between the observed and predicted trajectories. For example during trial 1 the observed and predicted displacements were about 80 km to the southwest. One week later during trial 2, the observed and predicted displacements were only 20 km and to the southeast.

[37] To quantify the skill of the model with respect to drifter position, let $\vec{x}_1^o(t)$, ... $\vec{x}_n^o(t)$ denote the observed positions of n drifters at time t and let $\vec{x}_1^p(t)$, ... $\vec{x}_n^p(t)$ denote the corresponding predictions. The median of $|\vec{x}_1^o(t) - \vec{x}_1^o(t_0)|$,... $|\vec{x}_n^o(t) - \vec{x}_n^o(t_0)|$ is a robust measure of the observed horizontal displacement of the n drifters with respect to their initial position at t_0. It can be interpreted as the radius of a circle which, when centered on the initial position of each drifter, will encompass 50% of the drifters at time t. The median is plotted as a function of time in Figure 7 for each of the four trials. The top left panel, for example, shows that after 100 hours, only half of the drifters are within about 100 km of their initial position; the bottom right panel shows in trial 4, half of the drifters moved less than 20 km in 100 hours. (A detailed description of drifter motion during each of the trials is given by Smith et al. [1998].)

[38] The median of $|\vec{x}_1^o(t) - \vec{x}_1^p(t)|$, ...$|\vec{x}_n^o(t) - \vec{x}_n^p(t)|$ is a robust measure of the error in the positions of the n drifters with respect to their predicted positions. This statistic is also plotted as a function of time in Figure 7 for each of the four trials. It can be interpreted as the radius of a circle which, when centered on the predicted position of each drifter, will encompass 50% of the drifters at time t. The top left panel of Figure 7 shows for example that after 100 hours, half of the drifters in trial 1 were within about 30 km of their predicted positions. Comparing the solid and dotted lines it is clear that the model has significant predictive skill for the two most energetic deployments, i.e., trial 1 and trial 3. For trials 2 and 4 the model prediction is not much better than the initial position.

[39] *Smith et al.* [1998] compared the skill of CANSARP, the operational marine and rescue planning tool for the region, against predictions based on the last known position, $\vec{x}^o(t_0)$, and the circulation model. They focused on the first 24 hours because this is the time period most relevant to search-and-rescue missions in the cold winter waters off the east coast of Canada. The CANSARP system is based on (i) background surface currents diagnosed from historical

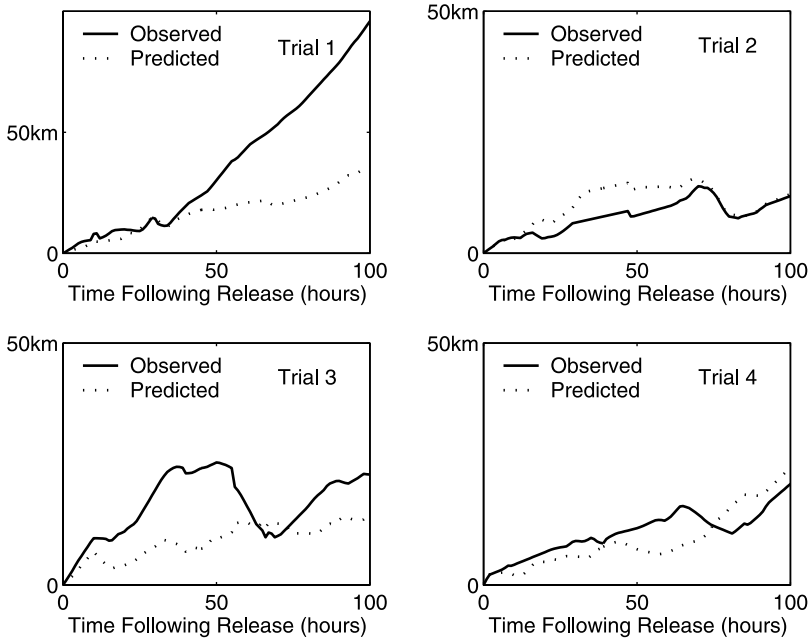

Figure 7. Horizontal dispersion (in kilometers) of the drifters through time for each of the four trials. The solid line shows the radius of a circle, which, when centered on the initial position of each drifter, will encompass 50% of the drifters at the time shown. The dotted line shows the radius of a circle, which, when centered on the positions predicted by the model, will encompass 50% of the drifters at the time shown. Note the different scale for trial 1.

near-surface current meter data, seasonally stratified; (ii) wind-driven flow calculated using Ekman theory or an empirical scaling and rotation of the wind; (iii) empirical, object-dependent, leeway factors published in the National Search and Rescue Manual. In the *Smith et al.* [1998] study the 35 km winds were used to drive an Ekman model [*Madsen*, 1977]. Note that the CANSARP leeway factors were consistently higher than those listed in Table 3. A major conclusion from the *Smith et al.* [1998] study was that the last known position is a significantly better predictor of subsequent drifter position over the first 24 hours than CANSARP for all trials except trial 3. Smith et al. also show that over the first 24 hours the circulation model outperformed CANSARP in all trials.

5. Sensitivity Studies

[40] The sensitivity of model predictions to changes in eddy viscosity, bottom friction and the horizontal resolution of the wind is now examined. Sensitivity is measured by the variance of the error in predicting alongshore current at 16 m midway between S2 and S3.

5.1. Vertical Eddy Viscosity and Bottom Friction

[41] *Csanady* [1982] gives the following empirical formula for the depth of a turbulent Ekman layer:

$$\delta_E = \frac{u_*}{10f} \tag{9}$$

where $u_* = \sqrt{\tau/\rho}$ is the friction velocity based on the wind stress magnitude τ. Applying this formula to the winds plotted in Figure 2 gives a mean Ekman depth of 10 m and a maximum depth of 23 m. This maximum corresponds to a vertical eddy viscosity of about 260 $cm^2\ s^{-1}$. This is smaller than the value of 650 $cm^2\ s^{-1}$ used by *Thompson and Sheng* [1997] and reflects the weaker winds observed in February 1996 compared to winter 1985–1986 [*Sheng et al.*, 2001].

[42] For the standard model run discussed in the previous section, we assumed base values of $k = 0.15$ cm s^{-1} and $\mu = 204$ $cm^2\ s^{-1}$. The latter corresponds to an Ekman depth of 20 m. The error variance for this case is Var(O-P) = 20.8 $cm^2\ s^{-2}$ (case 6, Table 4). Increasing the Ekman depth to 30 m (case 3, Table 4) did not improve the fit of the model significantly: the variance of the prediction errors decreased slightly from 20.8 to 20.1 $cm^2\ s^{-2}$. Changing the bottom friction coefficient had a more significant effect. Cases 4–7 show that increasing k from 0.05 to 0.20 cm s^{-1} decreases Var(O-P) from 24.5 to 20.2 $cm^2\ s^{-2}$. (Fitting a quadratic in k through these error variances leads us to conclude that the error variance for the optimal k is about 20 $cm^2\ s^{-1}$.)

5.2. Horizontal Resolution of Wind Field

[43] Increasing the wind resolution from 35 to 12 km did not increase the predictive skill of the circulation model. In fact the prediction error variance increased slightly (compare cases 6 and 8 in Table 4). We note however that the winds were relatively weak during February 1996 and that higher-resolution winds may prove more useful during stormier periods. *Smith et al.* [1998] also found that driving CANSARP with higher-resolution winds did not improve the predictions of drifter position.

Table 4. Summary of Sensitivity Studies Using the Barotropic model[a]

Case	Wind	μ, $cm^2\ s^{-1}$	k, cm s^{-1}	Var(O-P), $cm^2\ s^{-2}$	γ^2
1	35 km	460	0.05	24.2	0.74
2	35 km	460	0.10	21.4	0.65
3	35 km	460	0.15	20.1	0.61
4	35 km	204	0.05	24.5	0.75
5	35 km	204	0.10	22.0	0.67
6	35 km	204	0.15	20.8	0.65
7	35 km	204	0.20	20.2	0.61
8	12 km	204	0.15	22.2	0.72
9	Sable	204	0.15	25.9	0.79

[a]Cases 1–7 explore sensitivity to changes in the bottom friction coefficient k and eddy viscosity μ. The last two cases explore sensitivity to changes in the horizontal resolution of the wind.The column labelled Wind gives the horizontal resolution of the wind field used to force the model. The case labelled Sable corresponds to forcing by a spatially uniform wind field equal everywhere to that observed at Sable Island. Columns labelled μ and k show the eddy viscosities and bottom friction coefficients used in the sensitivity runs of the barotropic model. Var(O-P) is the variance of the difference in observed (O) alongshore currents averaged between moorings at 16 m depth, and the corresponding model prediction (P). γ^2 is the ratio of Var(O-P) to Var(O).

[44] As an illustration of the importance of resolving synoptic features in the wind field, we forced the model with a spatially uniform wind equal everywhere to that observed at Sable Island (case 9, Table 4). Given that Sable Island is about 400 km from the coast it is perhaps not surprising that the variance of the prediction errors increased from 20.8 to 25.9 $cm^2\ s^{-2}$.

6. Summary and Discussion

[45] A relatively simple model of near-surface, subtidal flow on the Scotian Shelf has been developed. The mean circulation is diagnosed from density observations and the time-varying component is calculated by a barotropic model forced by the local wind and sea level along the eastern boundary of the model domain. The skill of the model was assessed using an independent set of bottom pressure, current and drifter observations made on the inner Scotian Shelf in February 1996.

[46] The model gave reasonable predictions of alongshore flow on horizontal scales exceeding 15 km ($0.5 \leq \gamma^2 \leq 0.6$) and differences in bottom pressure across the inner shelf ($\gamma^2 = 0.5$). The model was less successful at predicting subtidal variations in alongshore flow at individual current meters. This is due in part to a mismatch in the spatial scales evident in the observations and the scales of motion resolved by the model. For example the correlation between near-surface, alongshore currents observed at moorings S2 and S3 is 0.4; the corresponding correlation for the predictions is 0.9. The model also failed to predict the strong cross-shelf currents that were observed during the field program. We speculate that the reason for these discrepancies is that the model density field does not evolve with the flow. Some support for this speculation comes from remotely sensed images of sea surface temperature [*Sheng et al.*, 2001], which show, for example, that the O(10 cm s^{-1}) cross-shelf flow observed during trial 1 coincided with the appearance of a gyre-like feature in the vicinity of the moorings with a scale of order 10 km.

[47] Skill in predicting drifter trajectories was measured by the median of the difference in observed and predicted position for a cluster of drifters. This statistic can be interpreted as the search radius, centered a predicted target position, that ensures a 50% chance of finding the search target. By combining all four trials we estimated a search radius of 6 km after 24 hours and 10 km after 48 hours. Using the initial position as the predictor of future position gave search radii that were more variable amongst trials and through time. In trial 3 for example the search radius centered on the initial position was about 25 km after 48 hours and then dropped to 10 km as the cluster of drifters moved back toward their release point over the next 20 hours. In contrast, the search radius centered on the model predictions increased almost linearly with time, outperforming the initial position at 48 hours and only managing to equal it 20 hours later. This illustrates the obvious point that persistence is a good predictor if the drifter returns to the release point; the problem of course is predicting when this will happen.

[48] Drifter trajectories predicted by the initial position and the circulation model were generally more accurate than those calculated by CANSARP over the first 24 hours. The circulation model may have benefited from a more accurate background flow and an improved set of leeway factors. It may also benefited from additional information on the propagation of remotely generated shelf waves along the shelf. It is important to note that the trajectories calculated using the circulation model were hindcasts that took advantage of all oceanographic data available for February 1966.

[49] We have speculated that the density field should be allowed to evolve with the flow in order to improve the predictions of cross isobath flow and the spatial structure in alongshore current. This will require a significant increase in model complexity and the assimilation of additional data such as sequences of satellite images of sea surface temperature and drifter trajectories, including those from drifters deployed by search agencies around the last known position of a person in water. Another improvement will come from the use of a larger-scale model, forced by forecast winds, that can provide forecast boundary conditions for a nested, high-resolution model. Both of these improvements are presently underway.

[50] **Acknowledgments.** The authors are grateful to Dr. Ken Drinkwater for kindly providing the hydrographic data, Dr. David Greenberg for the bathymetry, Dr Gilles Verner for help with the CANSARP calculations, Mr. A. Patterson for leeway factors and operational support, Ms. Judy St. James for preparing the high-resolution winds, and finally the two reviewers of the manuscript. This work was funded by the Canadian Coast Guard and NSERC through their Strategic Grants program.

References

Abramowitz, M., and I. A. Stegun, *Handbook of Mathematical Functions*, 1046 pp., Dover, Mineola, N.Y., 1970.

Chapman, D. C., Numerical treatment of cross-shelf open boundaries in a barotropic coastal ocean model, *J. Phys. Oceanogr.*, *15*, 1060–1075, 1985.

Csanady, G. T., The pressure field along the western margin of the North Atlantic, *J. Geophys. Res.*, *84*, 4905–4914, 1979.

Csanady, G. T., *Circulation in the Coastal Ocean*, 279 pp., D. Reidel, Norwell, Mass., 1982.

Csanady, G. T., The free surface turbulent shear layer, *J. Phys. Oceanogr.*, *14*, 14,402–14,411, 1984.

Madsen, O. S., A realistic model of the wind-induced Ekman boundary layer, *J. Phys. Oceanogr.*, *7*, 248–255, 1977.

Miller, M. J., and A. J. Thorpe, Radiation conditions for the lateral boundaries of limited-area numerical models, *Q. J. R. Meteorol. Soc.*, *107*, 615–628, 1981.

Oceans Ltd., Drift of common search and rescue objects—Phase III, *Transp. Can. Publ. TP 12179*, 184 pp., 1994.

Orlanski, I., A simple boundary condition for unbounded hyperbolic flows, *J. Comput. Phys.*, *21*, 251–269, 1976.

Sheng, J., and K. R. Thompson, A modified Galerkin-spectral method for three dimensional, barotropic, wind-driven shelf circulation, *J. Geophys. Res.*, *98*, 7011–7022, 1993.

Sheng, J., and K. R. Thompson, A robust diagnostic method for estimating surface circulation from vertical density profiles, *J. Geophys. Res.*, *101*, 25,647–25,659, 1996.

Sheng, J., K. R. Thompson, L. Cong, P. Smith, and D. Lawrence, Effect of wind and local density on the subtidal circulation on the inner Scotian Shelf, *Cont. Shelf Res.*, *21*, 1–19, 2001.

Smith, P. C., Validation procedures for oil spill trajectory models, *Can. Tech. Rep. Hydrogr. Oceanol. Sci.*, *140*, 168–183, 1992.

Smith, P. C., and F. B. Schwing, Mean circulation and variability on the eastern Canadian continental shelf, *Cont. Shelf Res.*, *11*, 977–1012, 1991.

Smith, P. C., D. J. Lawrence, K. R. Thompson, J. Sheng, G. Verner, J. St. James, N. Bernier, and L. Feldman, Improving the skill of search and rescue forecasts, *Can. Meteorol. Oceanogr. Soc. Bull.*, *26*(5), 119–129, 1998.

Thompson, K. R., and J. Sheng, Subtidal circulation on the Scotian Shelf: Assessing the hindcast skill of a linear, barotropic model, *J. Geophys. Res.*, *102*, 24,987–25,004, 1997.

Wright, D. G., D. A. Greenberg, J. W. Loder, and P. C. Smith, The steady-state barotropic response of the Gulf of Maine and adjacent regions to surface wind-stress, *J. Phys. Oceanogr.*, *16*, 947–966, 1986.

L. Cong, J. Sheng, P. C. Smith, and K. R. Thompson, Department of Oceanography, Dalhousie University, Halifax, Nova Scotia, Canada, B3H 4J1. (Keith.Thompson@Dal.Ca)